Numerical modelling of debris flows with large boulders

A dissertation by

Mario Germán Trujillo-Vela

Submitted to the Faculty of Engineering of
Pontificia Universidad Javeriana
in partial fulfilment of the requirements for the degree of
Doctor of Engineering

Pontificia Universidad
JAVERIANA
Bogotá

Faculty of Engineering
Pontificia Universidad Javeriana
Bogotá D.C., Colombia
February 2021

Advisors

Ph.D. Alfonso Mariano Ramos-Cañón
Full Professor, Department of Civil Engineering
Pontificia Universidad Javeriana, Bogotá D.C., Colombia
E-mail: a-ramos@javeriana.edu.co

Ph.D. Jorge Alberto Escobar-Vargas
Associate Professor, Department of Civil Engineering
Pontificia Universidad Javeriana, Bogotá D.C., Colombia
E-mail: jorge-escobar@javeriana.edu.co

Ph.D. Sergio Andrés Galindo-Torres
Associate Professor, School of Engineering
Westlake University, Hangzhou, China
E-mail: s.Torres@westlake.edu.cn

Declaration

I hereby declare that except where specific reference is made to the work of others, the contents of this dissertation are original and have not been submitted in whole or in part for consideration for any other degree or qualification in this, or any other university. This dissertation is my own work and contains nothing which is the outcome of work done in collaboration with others, except as specified in the text and Acknowledgements.

Mario G.

Understanding nature through science, even making use of artificial extensions of our senses, is a laudable purpose, but to comprehend life seems to be the most tender illusion that human being has ever had.

Mario G.

Dedication

To my parents Pastora Vela Carvajal and José Ricaurte Trujillo Carvajal because all the support and love never mind where I am.

Acknowledgement

The acknowledgements are organised chronologically.

Institutions:

Firstly, I would like to thank the Geophysical Institute at the Pontificia Universidad Javeriana for the economic support to assist some congresses and courses. Also, for giving me a workplace and the warmness of a home for seven years.

Second, I want to acknowledge the Fundación CeiBA –Bogotá– for providing me with the scholarship with which I could study my PhD.

Third, I acknowledge the University of Liverpool for providing me with a place and access to the high-performance computer to develop part of my thesis.

Fourth, I am greatly grateful for the economic support and facilities supplied by the Multi-Scale and Multi-Physics Modelling Laboratory (M3Lab) of the School of Engineering at the Westlake University – 西湖大学 – through the Visiting Student Program that allowed me to conclude my PhD studies. Also, because I could access the Super Computer that has been crucial for performing this thesis.

People:

I have deep gratitude to professor Alfonso Mariano Ramos Cañón, for encouraging me, being patient, all teachings and guidance I have been receiving since I arrived in Bogotá when I was finishing my undergraduate.

I acknowledge professor Jorge Alberto Escobar Vargas for guiding me since I started the master degree. The teachings, especially about numerical methods, have been crucial in my studies.

I am grateful to professor Sergio Andrés Galindo Torres for providing me with the guidance and standpoint of a physicist and allowing me to join him in two fascinating and important journeys through the world, in the United Kingdom and China. The cultural enrichment that I have gained during this time is invaluable.

It has been an exceptionally enriching experience from the academical standpoint to have the three of them as tutors simultaneously. I have enjoyed receiving advice and the discussions we had during all this time.

I acknowledge Dr José María González Ondina because he always had time to get into very interesting discussions about fluid mechanics.

I acknowledge Dr Maziar Gholami Korzani for the valuable discussions and the code

PersianSPH on which my thesis is based on.

I acknowledge professor Joan Manuel Larrahondo, also Lorena Beltran and John Sanchez –the latter who has passed away– for allowing me to perform collaboration, thus obtaining a publication.

I thanks all the people who have been a good company in each stage of this process and who have helped me when I have needed them, Andrés Clavijo, Paula Villegas, Nidia Reyes, Constanza Castelblanco, Karen Fernandez, Kunle Olaitan, 任松凯 and 葛转.

My deepest gratitude to Silvia Cabrera Díaz who took me like another son since I was in school.

Conference and journal publications related to this thesis

Trujillo-Vela, M. G., Galindo-Torres S. A., Zhang X., Ramos-Cañón, A. M., and Escobar-Vargas, J. A. (2020). "Smooth particle hydrodynamics and discrete element method coupling scheme for the simulation of debris flows." *Computers and Geotechnics*, 125,1–17.

Trujillo-Vela, M. G., Escobar-Vargas, J. A., and Ramos-Cañón, A. M. (2020). "A spectral multidomain penalty method solver for the numerical simulation of granular avalanches." *Earth Sciences Research Journal*, 23(4),171–183.

Trujillo-Vela, M. G., Galindo-Torres S. A., Zhang X., Ramos-Cañón, A. M., and Escobar-Vargas, J. A. "SPH-DEM coupling for debris flows." In XIV World Congress on Computational Mechanics (WCCM). In: Paris, France - Online. 11-15 Jan, 2021.

Contents

1 Introduction **1**

1.1 Debris flows phenomenology . . . 2

1.1.1 Rheology of debris flows . . . 4

1.1.2 Large boulders in debris flows . . . 5

1.2 Problem statement . . . 6

1.3 Aim . . . 7

1.3.1 Objectives . . . 7

1.4 Document outline . . . 8

2 Review of debris flow modelling **9**

2.1 Phases of the flow . . . 9

2.1.1 Single-phase models . . . 9

2.1.2 Mixture models . . . 10

2.1.3 Multiphase models . . . 11

2.2 Constitutive models . . . 11

2.2.1 Fluids . . . 11

2.2.2 Soils . . . 13

2.2.3 Debris flows . . . 13

2.3 Dimensionality . . . 14

2.3.1 3D models . . . 14

2.3.2 2D models . . . 14

2.3.3 1D models . . . 15

2.4 Numerical techniques . . . 15

2.4.1 Grid-based methods . . . 15

2.4.2 Mesh-free methods . . . 17

2.5 Summary and discussion . . . 19

3 Depth-integrated mesh-based Eulerian approach for debris flows **24**

3.1 Depth-integrated governing equations . . . 24

3.2 Depth-integrated dry granular flow 27
3.2.1 Numerical setup 27
3.2.2 Boundary conditions 29
3.2.3 The tracking of the free surface 30
3.2.4 Stability condition and mass conservation 31
3.3 Results of depth-integrated dry granular flow 32
3.3.1 Grid independence test 32
3.3.2 Analysis of boundary conditions 33
3.3.3 Analysis of lateral earth pressure coefficient, $k_{a/p}$ 37
3.3.4 Analysis of the momentum correction factor, β 38
3.4 Discussion 41

4 Multiphase mesh-free approach for debris flow 43
4.1 Multiphase mathematical modelling 43
4.1.1 Conservation equations 43
4.1.2 Multiphase processes 47
4.1.3 Constitutive equations 47
4.1.4 Interaction forces 55
4.1.5 Three-phase 3D governing equations 57
4.2 Mesh-free methods 59
4.2.1 Smooth Particle Hydrodynamics (SPH) 59
4.2.2 Discrete Element Method (DEM) 69
4.2.3 SPH-DEM coupling 71
4.2.4 General diagram of the code 75
4.3 Results of SPH-DEM coupling validation cases 77
4.3.1 Poiseuille flow 77
4.3.2 Square array of cylinders immersed in fluid 80
4.3.3 Dry granular flow impact on an immovable wall 84
4.3.4 Real scale dry landslide 88
4.4 Results of a hypothetical debris flow 93
4.5 Discussion 103

5 Conclusions and discussion 105
5.1 Depth-integrated grid-based approach 105
5.2 Multiphase mesh-free approach 106
5.3 General perspective 108

6 Future work 109

References **111**

A Tensorial calculus identities **130**

B SPH derivatives **133**

B.1 Derivative of a function . . . 133
B.2 Product rule and derived function . . . 134
B.3 Quotient rule and derived function . . . 135
B.4 Pressure or stress terms . . . 136
B.4.1 Square density pressure . . . 136
B.4.2 Multiplied density pressure . . . 137
B.5 Viscous terms . . . 137
B.5.1 Morris et al. (1997) viscosity . . . 137
B.5.2 Shao and Lo (2003) viscosity . . . 138
B.5.3 Takeda et al. (1994) viscosity . . . 139

List of Figures

1.1 Debris flow and colluvial fan relationship. 3
1.2 Large boulders photographed in different debris flow cases around the world. (a) Large boulder deposited adjacent to a building with a height similar to one floor of the construction, destroyed by a debris flow on December 14-16th, 1999, Vargas state, Venezuela (Larsen et al., 2002; Wieczorek et al., 2016). (b) Boulder transported in debris flow on December 14-16th, 1999, Vargas state, Venezuela, which size is 11.3x5.0x3.5 m (Wieczorek et al., 2016). (c) Large boulder with a diameter comparable to human size carried by a lahar event on May 18th, 1989 eruption in Mount St. Helens, Washington, United States. Photo by Lyn Topinka, USGS, September 16th, 1980. (d) Large boulders with a diameter similar to flow depth carried by the front of a debris flow in July 2016, Illgraben, Switzerland. Video recorded by (Zufferey, 2016). 3
1.3 Photographs of large boulders taken after a debris flow event occurred on March 31st, 2017, in Mocoa, Colombia. (a) Large boulder deposited on the bank of the Taruca creek with the size of 4x4x2 m. (b) Large boulders whose maximum size are 10.2 m and 7.4 m, from left to right, respectively. (c) Large boulders with a diameter comparable to human size deposited on the drainage line of the Taruquita creek. (d) Boulders deposited on the colluvial fan in Mocoa city, where the largest boulder has a maximum size of 9 m. 4
1.4 Sketch of large boulders in debris flows. 5

2.1 Rheological models. (a) Shear-stress and strain-rate relationship for fluids. (b) Viscosity behaviour as a function of the strain-rate. (c) Simple stress-strain relationships for soils. 12

3.1 Initial conditions used in shallowness approach. (a) 3D view of the topographic basis of an inclined curvilinear plane with a wedge-shaped initial condition, $\zeta = b + \mathbb{h}$. (b) cylinder. (c) Gaussian bump. 29
3.2 Reflective boundary conditions, a) slip and b) non-slip in the tangential direction. 30
3.3 Mass conservation error with a) slip and b) non-slip boundary conditions. (Sub_x and Sub_y represent the subdomain numbers in x and y directions, respectively). 33
3.4 Mass conservation error in function of time with and without average depth and no topographic gradient, a) Gaussian bump and b) cylinder. 33
3.5 a) Granular flow experiment. b) Numerical prediction given by SMPM for spatial refinement with low numerical error ($N = 8$, $Sub_x = 108$, and $Sub_y = 18$), slip boundary conditions, and constant lateral earth pressure coefficient. 34
3.6 a) Granular flow experiment. b) Numerical prediction given by SMPM for spatial refinement with low numerical error ($N = 8$, $Sub_x = 108$, and $Sub_y = 18$), non-slip boundary conditions, and constant lateral earth pressure coefficient. 35
3.7 Comparison between numerical results using SMPM and experimental data of the centroid of the moving mass and the velocity field. a) The position of the centroid of the descending mass at each time step. b) Centroid of the velocity field. V is the total volume. 37
3.8 a) Granular flow experiment. b) Numerical prediction given by SMPM for spatial refinement with low numerical error ($N = 8$, $Sub_x = 108$, and $Sub_y = 18$), slip boundary conditions, and regularized lateral earth pressure coefficient. 38
3.9 Comparison of the flow depth ($\mathbb{h}$) via a longitudinal profile in the flume centre at two time-steps, (a) $t = 0.10$ s, and (b) $t = 0.32$ s. Green dashed line is the experiment given by Denlinger and Iverson (2001), and the solid black line is the numerical prediction using SMPM for different β. 39
3.10 Comparison of the flow depth ($\mathbb{h}$) via a longitudinal profile in the flume centre at two time-steps, (a) $t = 0.53$ s, and (b) $t = 0.93$ s. Green dashed line is the experiment given by Denlinger and Iverson (2001), and the solid black line is the numerical prediction using SMPM for different β. 40
3.11 Comparison of the flow depth via a longitudinal profile in the flume centre at time $t = 1.50$ s. Green dashed line is the experiment given by Denlinger and Iverson (2001), and the solid black line is the numerical prediction using SMPM for different β. 41

4.1 Sketch of the three phases. Soil represented as a continuum (brown hatched body)-, fluid represented as a continuum (blue opaque body), and the boulders as discrete spheres (reddish circle). 58
4.2 Basic sketch of SPH interpolation. 60
4.3 Sketch of fluid-soil interaction force with SPH. 65
4.4 Coupling SPH-DEM scheme. (a) DEM sphere interacting with SPH particles. (b) DEM segments or planes are interacting with SPH particles. The blue particle represents the SPH particle, the purple particle is a virtual particle, and the circular and flat objects are DEM particles, whose positions are $\mathbf{x}_{sph}$, $\mathbf{x}_s$, and $\mathbf{x}_{dem}$, respectively. 71
4.5 Flow diagram of the computational code. 76
4.6 Sketch of SPH-DEM coupling for Poiseuille problem. 77
4.7 Vertical velocity profile comparison to the analytical solution (Equation 4.176). (a) SPH velocity obtained by the use of SPH boundary particles and (b) SPH velocity obtained by the use of DEM plates at the boundaries. 79
4.8 Comparison of the force profile (solid line) given by the analytical solution (Equation 4.179) to the numerical solution given by Equation 4.168 (blue triangles). 80
4.9 Euclidean norm of the error of the velocity profile as a function of time for both treatments at the boundary conditions, SPH dummy particles and DEM plates. 80
4.10 Euclidean norm of the error of the force obtained on the DEM plates as a function of the time. 80
4.11 Square array of cylinders (DEM particle) immersed in a fluid flow (SPH particles). Paths for comparison 3 and 4. 81
4.12 Flow around sphere DEM for a solid concentration $c = 0.125$ with periodic boundary conditions. (a) and (c) compare the velocity distribution (u, m/s) without and with δ-SPH filter, respectively. (b) and (d) compare the pressure field ($p - p_{mean}$, Pa) without and with δ-SPH filter, respectively. 82
4.13 Comparison of pressure produced by the SPH-DEM coupling to the solution given by FEM presented in Morris et al. (1997). 83
4.14 Comparison of the dimensionless permeability to the analytical solution taken from Sangani and Acrivos (1982); Adler (2013). 84
4.15 Initial condition of the dry granular material inside the flume. The gray and black planes are DEM objects and the brown box is composed of SPH particles. 85
4.16 Lateral view of the dry granular flow with a slope angle $\theta = 45°$. The colour map indicates the norm of the velocity vector $|\mathbf{u}|$ of the SPH particles. . . 86

4.17 Comparison of the impact force obtained from the experiment of the dry granular flow generated by Moriguchi et al. (2009), and the SPH-DEM simulation. 87
4.18 Comparison of the peak impact force obtained from the experiment of the dry granular flow generated by Moriguchi et al. (2009), the numerical results from He et al. (2018), and the solution provided by the coupled SPH-DEM. 87
4.19 (a) Yangbaodi landslide occurred in China in 2002. Photography taken from Li et al. (2012). (b) Initial configuration of the Yangbaodi landslide. Three tracking points (green points A, B and C). 89
4.20 (a) Initial mass distribution of the dry landslide using SPH boundary conditions. (b) solution at $t = 30$ s with SPH BC. 90
4.21 Norm of the velocity vector $|\mathbf{u}|$ of soil SPH particles going down the slope using DEM boundary conditions. 91
4.22 Comparison between SPH and PFEM. The solid green and dashed blue line are the velocity of the tracked point, A, B and C given by PFEM and SPH-DEM, respectively. The left and right–hand side column give the velocity in the x and y direction, respectively. The dashed red line represents the path of the tracked points. The solid black line represents the topography. The dotted grey and solid fuchsia lines are the final deposit shape obtained by PFEM and SPH-DEM, respectively. 92
4.23 Initial configuration of the fluid and soil SPH particles, and DEM boulders (fuchsia points). Three soil SPH particles are tracked during the movement (green points A, B and C). 94
4.24 Hydrograph of the inlet flow. 94
4.25 Norm of the velocity vector $|\mathbf{u}|$ of SPH soil particles and DEM boulders going down the slope. 96
4.26 Norm of the velocity vector $|\mathbf{u}|$ of SPH soil particles and DEM boulders going down the slope. 96
4.27 Pore fluid pressure during the displacement of the entire mass and boulders (fuchsia points). 97
4.28 Pore fluid pressure during the displacement of the entire mass with no boulders. 98

4.29 Comparison between dry landslide and debris flow with and without boulders. The solid orange line and dotted green line represent the velocity of the tracked point, A, B and C given by the debris flow, with and without boulders, respectively. The dashed blue line shows the velocity of the tracked point, A, B and C given by the dry landslide produced with SPH in Section 4.3.4. The left and right–hand side column give the velocity in the x and y direction, respectively. The grey hatched area is the profile of the final deposit of the fluid-soil mixture in addition to the boulders (fuchsia points). 100
4.30 Energy versus time of each boulder during the flow. (a) potential energy. (b) kinetic energy. 101
4.31 Scheme of the control volume to measure the kinetic energy as a function of time. 101
4.32 Measurement of the kinetic energy at the distance of $x = 193.1$ m for the entire depth of the flow with boulders (black line) and with no boulders (blue line). 102

List of Tables

2.1 List of mathematical models for propagation of mass movements. 22

3.1 Value of the properties of the materials used in the numerical modelling. Taken from Denlinger and Iverson (2001). 29

3.2 Euclidean norm of the error for slip and non-slip SMPM, and for HLLC, regarding the experimental data. 35

4.1 Drucker-Prager parameters. 52

4.2 Parameter to reproduce the experiment of the dry granular flow. 85

4.3 The main differences of SPH models used to solve the impact force problem. 88

4.4 Parameter to reproduce the Yangbaodi landslide in dry conditions. Taken from Zhang et al. (2015); Li et al. (2012). 90

4.5 Debris flow parameters. 95

Nomenclature

Operator symbols

d	Total derivative
D	Material or Lagrangian derivative
∂	Partial derivative
Δ	Discrete increment or interval, discrete derivative
$\boldsymbol{\nabla}$	Nabla operator
$\int$	Integral
$\sum$	Summation
$\dot{( )}$	Time derivative
$() \cdot ()$	Dot product, inner product
$() : ()$	Double inner product, double contraction

Latin symbols

$\mathbf{a}^{fs}$	Acceleraction exerted on fluid from soil
$\mathbf{a}^{sf}$	Acceleraction exerted on soil from fluid
c	Cohesion of soil
c_s	Speed of the sound
d_m	Mean diameter of the supporting matrix
D_B	Diameter of large boulders
D_h	Hydraulic diffusivity
$\dot{\boldsymbol{e}}$	Deviatoric strain-rate tensor
$\boldsymbol{e}$	Deviatoric strain tensor
E	Young's modulus or bulk modulus of soil
E_K	Kinetic energy
E_P	Potential energy
$\mathbf{f}^{seepage}$	Seepage force
$\mathbf{F}$	Force vector
$\mathfrak{F}$	Total force vector
$\mathbf{F}^k$	Interaction force vector among phases
$\mathbf{F}^{fN}$	Force exerted on fluid from Boulders

$\mathbf{F}^{sN}$	Force exerted on soil from Boulders	
$\mathbf{F}^{Np}$	Force exerted on boulders from any other phase	
$\mathbf{F}(\mathbf{q}) = (F_1, F_2, F_3)$	Flux vector of the conservative variables	
$\mathbf{g} = (g_x, g_y, g_z)$	Gravitational acceleration vector	
g	Gravitational Constant	9.81 m/s^2
G	Shear modulus	
G_n	Normal viscous coefficient	
$\mathbf{G}(\mathbf{q}) = (G_1, G_2, G_3)$	Flux vector of the conservative variables	
$\mathbb{h}$	Depth of the flow	
h	Smoothing length	
H_o	Average depth of the flow	
$\mathbf{I}$	Moment of inertia tensor	
I_1, I_2, I_3	First, second and third invariant of the stress tensor	
J_2	Second invariant of the deviatoric stress tensor	
k	Intrinsic permeability	
k_f	Inertial permeability	
k_h	Hydraulic conductivity	
k_c	Drucker-Prager parameter	
$k_{a/p}$	Lateral earth pressure coefficient	
k_a	Active lateral earth pressure coefficient	
k_p	Passive lateral earth pressure coefficient	
k_{nat}	Natural or constant lateral earth pressure coefficient	
K	Elastic bulk modulus	
K_n	Stiffness coefficient	
m	Mass	
m_x, m_y	Conservative variables in x and y direction	
n	Porosity	
$\mathbf{n}$	Unit normal vector	
p	Pressure	
p_0	Reference pressure	
P_{bed}	Linear variation of fluid pressure	
q	Relative ditance between two points	
$\mathbf{q} = (q_1, q_2, q_3)$	Conservative variables vector	
$\mathbb{q}$	Sources and sinks of mass, entrainment rate of mass	
R_B	Radius of the boulder	
R_T	Artificial pressure for tensile inestability	
$\boldsymbol{s}$	Shear stress tensor for soils	
S	Surface area of the control volume	

$\mathbf{S(q)} = (0, S_x, S_y)$	Vector of source terms
t	Time
$\mathbf{t}$	Surface stress
$\mathbf{T}$	Torque
$\mathbf{u} = (u, v, w)$	Velocity vector
$\bar{\mathbf{u}} = (\bar{u}, \bar{v})$	Depth-integrated velocity vector
$\mathbf{u}_{rel}$	Relative velocity between SPH and DEM particles
U	Magnitude of depth-integrated velocities
$\mathcal{V}$	Control volume
W	Smoothing function or kernel
$\mathbf{x} = (x, y, z)$	Space coordinates

Greek symbols

α_c	Drucker-Prager parameter
α_k	Volumetric fraction of any phase
α_f	Volumetric fraction of fluid
α_s	Volumetric fraction of soil
α_Π	Artificial viscosity parameter
β	Momentum correction factor
β_Π	Artificial viscosity parameter
Γ	Tolerance value
$\boldsymbol{\delta}$	Kronecker delta
ϵ	Thickness of the sphero-polyhedra halo
$\boldsymbol{\varepsilon}$	Strain tensor
$\dot{\boldsymbol{\varepsilon}}$	Strain-rate tensor
ε_r	Coefficient of resitution
η	Kinematic viscosity
θ	Inclination angle
ϑ	Bulk modulus of fluid
ι	Initial pore pressure ratio
κ	Scaling factor of spread of the smoothing function
λ	Plastic multiplier
$\dot{\lambda}$	Rate change of plastic multiplier
$\mathit{\Lambda}$	Ratio of the basal pore fluid pressure
μ	Dynamic viscosity
ν	Poisson ratio
ξ	Displacement of the free surface
$\mathit{\Pi}$	Artificial viscosity variable
ρ	Density

ρ_0	Initial or reference density
σ_0	Yield stress
$\boldsymbol{\sigma}$	Total stress tensor
$\boldsymbol{\sigma}_f$	Total stress tensor of fluid
$\boldsymbol{\sigma}_s$	Total stress tensor of soil
$\boldsymbol{\sigma}'_s$	Effective stress tensor of soil
$\boldsymbol{\tau}$	Shear stress tensor of fluids
τ_0	Yield shear stress
Υ	Adiabatic exponent
ϕ	Angle of shearing resistance
ϕ_{int}	Internal angle of shearing resistance
ϕ_{bed}	Basal angle of shearing resistance
ψ	Dilatancy angle
Ψ	Steepness value of smoothing function
$\dot{\boldsymbol{\omega}}$	Vorticity or rotation-rate tensor
$\boldsymbol{\Omega}$	Angular velocity vector

Abbreviations

BC	Boundary Conditions
CFL	Courant-Friedrichs-Lewy stability condition
D	Dimensions
DEM	Discrete Element Method
DG	Discontinuous Galerkin
EOS	Equation of State
FDM	Finite Difference Method
FEM	Finite Element Method
FVM	Finite Volume Method
HLLC	Harten-Lax-van Leer-Contact Method
SMPM	Spectral Multidomain Penalty Method
SPH	Smooth Particle Hydrodynamics
δ-SPH	Delta Smooth Particle Hydrodynamics
WCSPH	Weak Compressible Smooth Particle Hydrodynamics
SPH-DEM	Coupled SPH and DEM method
Re	Reynolds number

Abstract

This work presents a broad insight into debris flows modelling by identifying their most relevant aspects and the changes proposed through time, offering a guideline to select models for simulating debris flows. Two of the most general standpoints are implemented and analysed for modelling debris flows, highlighting their advantages and weaknesses through the document. First, the performance of a specific spectral element-based technique with the Eulerian approach is verified using a standard depth-integrated set of debris flow equations for the first time. Second, the Lagrangian approach is used to propose a modelling framework suitable to study debris flows containing "three" phases. Fluid and soil phases are treated from the continuum standpoint, whereas the third phase is employed to represent large boulders treated like a different phase using the discontinuous approach. Large boulders with a size similar to the flow depth are found in debris flows deposits with a certain regularity. Although they are scarce in quantity, because of their size, such boulders can potentially play an essential role in the dynamics of debris flow, causing damage in infrastructure and obstructing the drainage lines when the events occur. A coupling strategy between Smooth Particle Hydrodynamics representing fluid-soil mixtures and the Discrete Element Method to include large boulders into the mass is also proposed. Thus, it is possible to connect the behaviour at very different scales in a unified framework more suitable to describe debris flows heterogeneity, using a three-phase model for the first time. The numerical coupling is validated using some cases reported in the literature, showing satisfactory results compared to analytical, numerical and field data.

Chapter 1

Introduction

The processes that occur on the earth surface, known as mass movements, may include multiple materials. The materials can be fluids (liquid and gas) and solids (clastic sediments and logs, for instance). Sediments have a broad spectrum of characteristics because of the mineral composition, shape and size of particles. Thus, fine- or coarse-grained soils, as well as the presence of boulders, may affect mass behaviour (Hungr et al., 2005; Takahashi, 2014). The mass movements are driven by gravity and generated by certain unfavourable conditions that can be classified as internal and external. The internal conditions are defined by the mechanical state of the ground, which can be expressed through several variables and parameters (e.g., morphology, stress, strain, angle of shearing resistance, apparent effective cohesion and pore pressure). External conditions are those that can produce changes of that state of the ground, such as weather, anthropic influences/actions, volcanic and seismic activity, amongst others.

Classification charts of the mass movement have been proposed based on the characteristics with which they are developed, such as the morphology of the movement (e.g., slides, falls, tumbles and flows), type of materials, solid-fluid ratio, velocity, transported volume and even source (Hutchinson, 1968; Varnes, 1978; Pierson and Costa, 1987; Coussot and Meunier, 1996; Hungr et al., 2001; Jakob, 2005b). There are several mass movements catalogued within the flow type. For instance, debris flows have special attention in research due to their high potential of damage since they can travel long distances, destroying everything on their path (Iverson, 1997; Hilker et al., 2009; Chen et al., 2014). These flows are the pivotal topic in this work; consequently, the most relevant phenomenological aspects will be presented below.

1.1 Debris flows phenomenology

Debris flows initiate with one or multiple slope movements, and ends with the deposition (Iverson, 1997). Also, they have a wide variability of materials, high content of water, high velocities and volumes. The water-sediment interaction processes (e.g., collision, friction, drag and viscosity) dominate the behaviour of the flow (Campbell, 1990; Pouliquen et al., 2006; MiDi, 2004). The main characteristics that have been identified during debris flows are:

- Segregation and recirculation of the materials due to the particle size, density and friction (Takahashi, 2014; Iverson, 1997; Gray and Thornton, 2005; Gray and Chugunov, 2006; Gray and Ancey, 2011; Leonardi et al., 2015).
- The volume will increase during the entrainment of materials to the flow due to the erosion of ground and banks (Hungr and Evans, 2004).
- Large boulders are transported by a finer matrix (Takahashi, 2014).
- Lateral levees are part of the deposition stage as a consequence of the "attempt" of escaping lateral confinement (Iverson, 2014).
- Colluvium fan or "lobe" is the zone where the most significant part of the flow is deposited by the friction of the mass (Jakob, 2005a; Regmi et al., 2015).

The entrainment of materials caused by the fast erosion produced during debris flows is crucial because of the volume change. The initial small volumes can be transformed into large ones by the entrainment of mass along the path. Such variation can be by several orders of magnitude (Hungr et al., 2005; Berger et al., 2011). For instance, Hungr and Evans (2004) report several cases of rock avalanches, where the initial volume increased by 2.5 or 10 times. Kaitna et al. (2013) reports increments in volume from 3 to 53 times in many debris flows field events. A more recent case of debris flow occurred on March 31st, 2017, in Mocoa (Colombia), with an approximate increment in volume of 7.5 times the initial mass (Prada-Sarmiento et al., 2019). The main two sources of mass entrainment are bed destabilisation and erosion, as well as instability of the stream banks, undercut by bed erosion (Hungr et al., 2005).

Bed and channel banks can be formed from other sediment transport processes or, more specifically, by the deposition of previous debris flow events. Debris flow deposition occurs at the base of steep slopes, which typically merge with valleys and water bodies, and it is recognised as colluvial fan (Jakob, 2005a; Regmi et al., 2015). Such deposition can be formed in two ways, through levees when the front of the flow is still moving and lobes when the motion is halted completely (Iverson, 2014). Thus, debris flows and colluvial fans can supply sediments to each other as a cycle that might have a particular frequency (Figure 1.1). Big boulders are also part of this process, deposited on levees and fans, and can be dragged again in new events (Blackwelder, 1928; Takahashi, 1981; Costa, 1984; Beaty, 1989; Takahashi, 2014; Iverson, 2014).

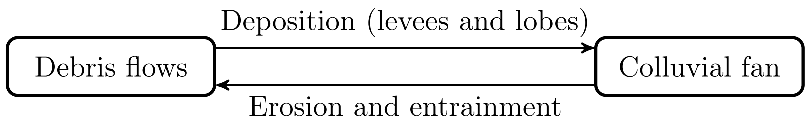

Figure 1.1: Debris flow and colluvial fan relationship.

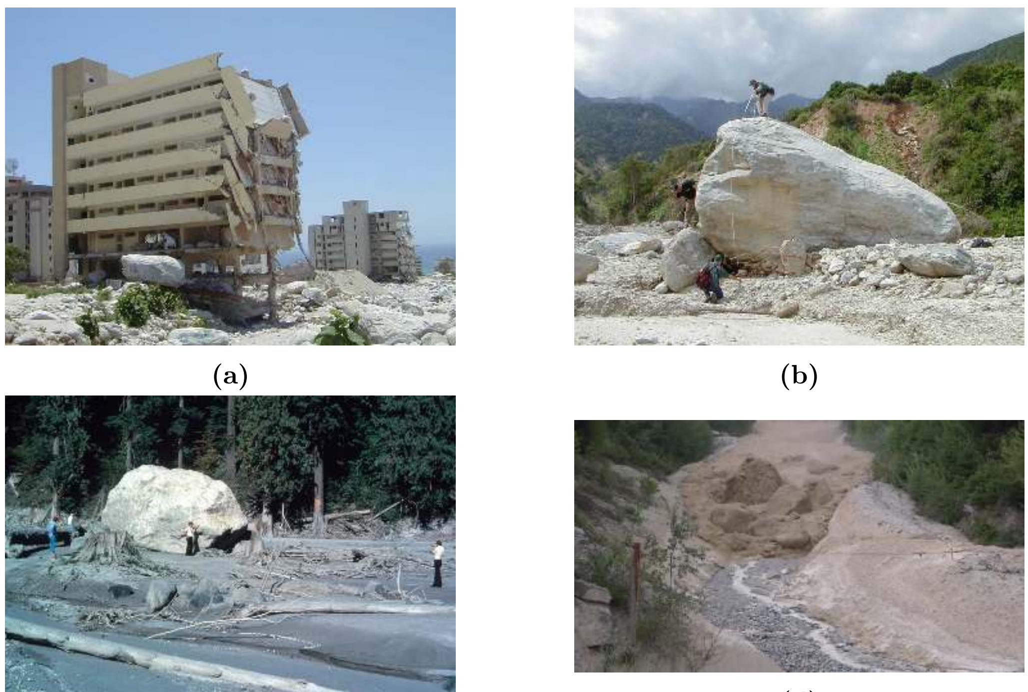

(a) (b) (c) (d)

Figure 1.2: Large boulders photographed in different debris flow cases around the world. (a) Large boulder deposited adjacent to a building with a height similar to one floor of the construction, destroyed by a debris flow on December 14-16th, 1999, Vargas state, Venezuela (Larsen et al., 2002; Wieczorek et al., 2016). (b) Boulder transported in debris flow on December 14-16th, 1999, Vargas state, Venezuela, which size is 11.3x5.0x3.5 m (Wieczorek et al., 2016). (c) Large boulder with a diameter comparable to human size carried by a lahar event on May 18th, 1989 eruption in Mount St. Helens, Washington, United States. Photo by Lyn Topinka, USGS, September 16th, 1980. (d) Large boulders with a diameter similar to flow depth carried by the front of a debris flow in July 2016, Illgraben, Switzerland. Video recorded by (Zufferey, 2016).

Large boulders found after some specific debris flow events, as shown in Figure 1.2. Figures 1.2a and 1.2b show boulders up to 11 m large found after a series of debris flows induced by a rainstorm which occurred on December 14-16th, 1999, along the northern coastal state of Vargas, Venezuela (Larsen et al., 2002; Wieczorek et al., 2016). Figure 1.2c shows a large boulder carried by a lahar event that occurred in a volcanic eruption on May 18$^{\text{th}}$, 1989, in Mount St. Helens, Washington, United States. Moreover, Figure 1.2d shows boulders carried on the front of a debris flow which happened in July 2016, in Illgraben, Switzerland (Zufferey, 2016).

During the debris flow in Mocoa, Colombia, boulders between 1 and 2 m in diameter were a significant part of the deposited mass on the colluvial fan. Besides, several large boulders whose longest side was about 4 to 10 m, were observed along the drainage line of the Taruca creek (Figures 1.3a-1.3c) and on the colluvial fan (Figure 1.3d). It is possible to see the importance of the entrainment of mass in debris flows, but the size of the incorporated materials also has a crucial role. Then, the primary question is, how do those large boulders are transported by debris flows. Some observations and suggestions are exposed below.

(a)

(b)

(c)

(d)

Figure 1.3: Photographs of large boulders taken after a debris flow event occurred on March 31$^{\text{st}}$, 2017, in Mocoa, Colombia. (a) Large boulder deposited on the bank of the Taruca creek with the size of 4x4x2 m. (b) Large boulders whose maximum size are 10.2 m and 7.4 m, from left to right, respectively. (c) Large boulders with a diameter comparable to human size deposited on the drainage line of the Taruquita creek. (d) Boulders deposited on the colluvial fan in Mocoa city, where the largest boulder has a maximum size of 9 m.

1.1.1 Rheology of debris flows

The wide variety of materials that are present in debris flows is what makes them so complex. Depending on the type of materials present in the mass can change the flow behaviour radically from muddy flows where fine particles form up the most significant part of the flow up to stony debris flows, where boulders with important size are the primary component of the phenomenon. The interaction forces among the materials produce the essential role of the movement of the mass. (1) Viscous forces in the fluid phase, (2) friction and collision among the solid participles and (3) pressure and drag forces between the solid and fluid phase are the fundamental identified forces given in such phenomena. The interaction forces are the crucial characteristics to be included in models that allow to study and identify other generalities of debris flows.

1.1.2 Large boulders in debris flows

It is possible to say that the diameter of large boulders D_B is much larger than the diameter of supporting matrix grains d_m, i.e., $D_B \gg d_m$. The diameter of big boulders is similar to the depth of the flow $\mathbb{h}$, i.e., $D_B \sim \mathbb{h}$. Also, the maximum reported size of large boulders in debris flows is about $D_{B(\max)} \approx 11$ m (Beaty, 1989; Iverson, 2014; Takahashi, 2014; Larsen et al., 2002). It has been noticed that the coarsest materials in a debris flow (e.g., gravel, cobbles and large boulders) accumulate on the surface (apparently "floating"), flowing towards the front of the flow (Takahashi, 2014; Hutter et al., 1994). Also, Takahashi (2014) ensures that if these big boulders are far larger than the neighbouring sediments and their size is comparable to the flow depth; they cannot be into the rear part of the flow.

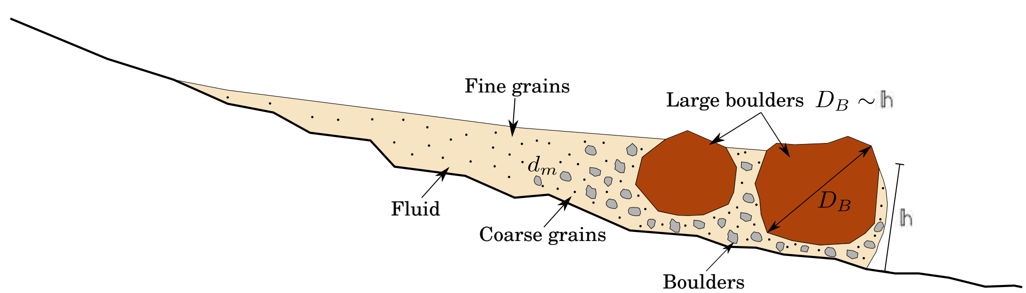

Figure 1.4: Sketch of large boulders in debris flows.

Some authors have tried to explain the phenomenon of transferring the larger particles towards the surface of the flow, referred to as inverse grading or segregation. Bagnold (1968) suggests the concept of dispersive pressure, caused by grain collision, which is proportional to the square of particle diameter, suggesting that larder particles will suffer higher dispersive pressure, being pushed toward the free surface. Another hypothesis says that the finer particles fell into the voids among coarser particles resulting in a relative ascent of coarser particles, known as dynamic sieving (Middleton, 1970). The idea given by Middleton (1970) has been disproved due to the disregard of the contemplation of particles density opposite to Bagnold's estimation (Sallenger, 1979; Takahashi, 2014).

A relevant characteristic is that the velocity profile varies from a minimum on the bottom to the highest on the free surface. Thus, once the most massive particles are on the top, they can move faster until they reach the front and fall to the bed again. Then, coarse particles can be buried by the flow or dragged in again, forming a recirculation of materials (Gray and Thornton, 2005).

Another observation is that, when the boulders are on the front, they tumble while being pushed by the rear part of the flow (Takahashi, 2014) (also, see video recorded by Zufferey (2016)). "Turbulent"[1] debris flows can transport large boulder as well. However, they are transported sporadically and do not accumulate at the front, and they are deposited in a scattered way in the colluvial fan (Takahashi, 2014). Different concepts such as cohesive strength, buoyancy, and structural support have been pointed out to explain how big boulders are supported on freshly deposited debris flow, although no further analysis was performed (Costa, 1984).

Some aspects whereby it is relevant to include large boulders in the modelling of debris flows and study their influence are: To know their potential to produce damage in structures, as shown in Figure 1.2c. The construction of barriers to mitigate the hazard of future debris flows requires both fluid pressure and the impact force of individual boulders (Banihabib and Forghanib, 2017). Boulders with such size sometimes are deposited in drainage lines (see Figure 1.3b-1.3c), which might facilitate the obstruction of the debris flows, producing temporal damming of water and sediments upstream. Such temporal natural dams can become more hazardous events after their failure.

The studies mentioned above highlight some attempts to understand the interaction between large boulders and the fluid-soil mixture in debris flows. However, there is no consensus on the processes and explanations. Hence, further studies using experimental, analytical and numerical strategies are warranted.

1.2 Problem statement

The previous mentioned phenomenological aspects have been identified by collecting field and experimental data. Many authors have then proposed mathematical models based on the conservation laws to reproduce debris flows (Savage and Hutter, 1989; Iverson and Denlinger, 2001; Pudasaini, 2012). The complexity of the models has been increasing during the last decades, being possible to study in a more specific way some aspects of debris flows. However, a great effort in understanding debris flows is still needed. One of the most relevant aspects of debris flows that have been poorly studied and understood is

[1] The Reynolds number is defined as $\mathrm{Re} = U\mathbb{h}/\eta$, where U is the cross-sectional mean velocity of the flow, $\mathbb{h}$ is the depth of the flow, and η is the kinematic viscosity of the interstitial fluid. If $\mathrm{Re} > 1500$ the debris flow is considered as turbulent (Takahashi, 2014).

the inclusion of large boulders in such flows.

Numerical tools are widely employed to study debris flows behaviour and their effect. A first attempt to incorporate such large boulders into debris flows numerical simulation have been presented in Martinez (2009). It was employed and presented the traditional depth-integrated[2] approach in the conservation equations with a Bingham fluid and the Discrete Element Method to represent large boulders. However, the depth-integrated approach does not allow the study of the verticality of the phenomenon, which might be relevant to observe some processes given in such a direction. Other couplings between the three-dimensional continuum phase and discrete elements have been developed to study the interaction between the fluid and granular phase (Tan and Chen, 2017; Xu et al., 2020; Leonardi et al., 2015; Liu et al., 2018). Nevertheless, such an approach requires a massive number of particles to represent the granular phase of debris flows being inconceivable in field-scale, as mentioned by Leonardi (2015).

It is why an appropriate modelling framework is indispensable to study such a specific phenomenon. Therefore, it is considered that the below described modelling setup might adequately reproduce debris flows that include large boulders. Fluid and soil can be represented with two phases model –hence two constitutive relationships– through the continuum approach, whereas the large boulders can be treated as a "third" phase using the Discrete Element Method. Thus, the present work contributes with a modelling framework that allows studying the dynamic interaction between large boulders and the whole "supporting" matrix of debris flows through the objectives presented as follows.

1.3 Aim

The main objective of this thesis is to propose a modelling framework that accounts for fluid, soil and large boulders for debris flow simulations. Such an aim will be achieved through the following objectives.

1.3.1 Objectives

1. To verify the performance of an existing mesh-based numerical technique to simulate debris flows.

2. To develop a coupling strategy between two specific mesh-free methods for describing the interaction among boulders and the supporting matrix.

[2]Depth-integrated, shallow water or shallowness approach are terms that can be found in the literature to refer to a type of equations obtained from the three-dimensional conservation equations after integrating them in depth. It will be better explained in Chapter 2, and these terms will be used in this document as synonyms.

3. To validate the numerical coupling of the mesh-free techniques.

1.4 Document outline

This thesis has been organised as follows: Chapter 2 presents the state of the art of modelling standpoints used in debris flows and emphasises the numerical techniques implemented to simulated such phenomena. It also offers a guideline for choosing models to reproduce debris flows. Chapter 3 shows the model, numerical setup and solution of a dry granular flow using a mesh-based Eulerian approach to verify the performance of a spectral element base technique, accomplishing objective 1. Chapter 4 presents the three-dimensional multiphase model from the Lagrangian approach, which contains the following main sections: Section 4.1 presents the development of the multiphase model in a detailed manner contributing directly to the aim of this thesis. Section 4.2 introduces the mesh-free numerical methods and their coupling, fulfilling the objective 2. Section 4.3 shows the validation cases of the coupled numerical methods that contribute to objective 3. Section 4.4 presents a hypothetical debris flow with all the materials demonstrating the potential of the proposed modelling framework. Chapters 5 and 6 shows conclusions and future work, respectively.